Constraining Absolute Higgs Couplings using Vector Boson Fusion $H \to WW$ with FCC-hh

Elliot Lipeles[1*] and Birgit Stapf[2*]

[1]University of Pennsylvania, Philadelphia, PA, USA.
[2]CERN, Geneva, Switzerland.

*Corresponding author(s). E-mail(s): lipeles@sas.upenn.edu; birgit.stapf@cern.ch;

Abstract

The absolute normalization scale of Higgs couplings is difficult to determine in hadron colliders. An experimentally and theoretically clean way to establish the coupling scale is to measure the ratio of resonant Vector Boson Fusion $\boldsymbol{H \to WW^*}$ production to non-resonant $\boldsymbol{qq \to qqWW}$ because both the theoretical and detector response systematics all cancel to first order in the ratio. To set the scale of the sensitivity, a simple selection and fit is presented with gives a 1.8% (1.9%) statistical uncertainty on the ratio for a 100 (84) TeV FCC-hh at 30 ab^{-1}, which would give a corresponding uncertainty on the $\boldsymbol{\kappa}$ scale of 0.5-1% depending on systematic effects and potential impacts of more sophisticated analysis.

1 Introduction

Hadron colliders can produce a large sample of Higgs bosons, but their precision is limited by our knowledge of several factors: PDF and luminosity uncertainties, calculational challenges of QCD, detector simulation, and background estimation. For example reference [1] shows statistical power to measure Higgs couplings at FCC-hh of order 0.5% for several couplings, but systematic limitations limit the precision to the 1.5-2% range. The impact of the systematic uncertainties can be mitigated by using ratios where some of these uncertainties cancel. These ratios then limit ratios of Higgs-couplings but leave the absolute scale of the couplings unconstrained. In some models, for example, a singlet mixing with the Higgs can lead to an overall suppression of Higgs couplings without modifying the ratios of couplings [2, 3].

There are ratios that can be taken between Higgs and other electroweak processes that provide absolute normalizations. Reference [4] presents ratios involved associated Higgs production WH to electroweak diboson production WZ. The ratio Vector Boson Fusion (VBF) production of Higgs to $WW \to e\nu\mu\nu$ over non-resonant VBF $qq \to WW \to e\nu\mu\nu$ provides an exceptionally clean example because the protons are coupling to vector boson with similar kinematics in both cases. The only differences are in the mass scale and spin of the produced system. Furthermore, the final state is identical except for the orientations and moderate differences in the energy scale of the observed particles. The combination of these means that the PDF, luminosity, QCD, and detector simulation uncertainties should cancel to a high degree; leaving the statistical and background estimation uncertainties likely to be dominant. The different-flavor, $e\nu\mu\nu$, final state is selected to avoid a large Drell-Yan background. This note presents a simple estimation of the background level and statistical power of such a measurement.

2 Samples

Madgraph [5] is used to simulate proton-proton collisions at 84 TeV and 100 TeV. Two signal processes are simulated VBF WW production via an s-channel Higgs boson and VBF WW production excluding diagrams with the Higgs boson, both with the W pair decaying fully leptonically. The two main backgrounds to this process are $t\bar{t}$ where both Ws in the top-quark decays decay leptonically, and $Z \to \tau\tau$ where the τ leptons decay to e or μ leptons. Pythia [6] is used to simulate the parton shower and DELPHES [7] with the FCC-hh scenario II card [8] is used to simulate the detector response. The processes shown in Figures 1a, 1b, and 1c are all generated in one sample requiring $pp \to jj\ell\nu\ell\nu$ with an s-channel Higgs Boson. The on-shell Higgs part is then separated based on the generated parton-level 4-lepton mass. The sample is normalized so that the produced rate in the 4-lepton mass peak is the 69 pb^{-1} on-shell VBF Higgs production cross-section calculated at NNLO-QCD and NLO-EWK[9]. The processes in Figures 1d and 1e are generated as $pp \to jj\ell\nu\ell\nu$ with QED=6 and with no Higgs or top in the diagrams. This means that the t-channel diagram and the interference of the two Higgs and Z process is not included which would have some effect, but not substantial compared to the level of precision presented. The $Z \to \tau\tau$ samples are generated with two jets above 80 GeV are normalised to the NNLO calculation of the cross-section using the NNPDF3.0 NNLO pdf [10].

3 Event Selection

The event selection uses a small set of standard VBF selection and top background suppression requirements to select for both Higgs to $WW \to e\nu\mu\nu$ and non-resonant VBF $qq \to WW \to e\nu\mu\nu$, specifically focusing on the final state with different lepton flavours to avoid Drell-Yan background with mismeasured missing transverse energy ($E\!\!\!/_{\mathrm{T}}$). The selection requires two jets with $p_T > 100$ GeV and no additional jets with $p_T > 30$ GeV, which acts as a simple central-jet veto for the VBF signature. The two jets are required not to pass the loose b-tagging requirements to suppress

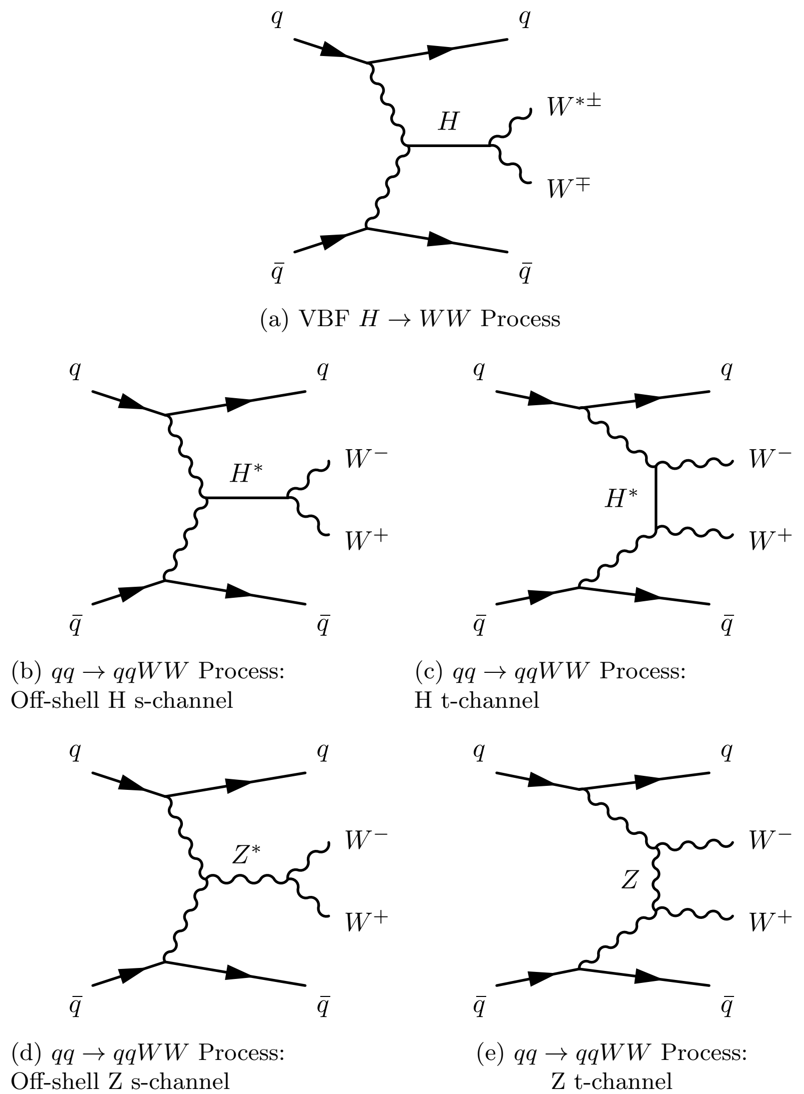

(a) VBF $H \to WW$ Process

(b) $qq \to qqWW$ Process: Off-shell H s-channel

(c) $qq \to qqWW$ Process: H t-channel

(d) $qq \to qqWW$ Process: Off-shell Z s-channel

(e) $qq \to qqWW$ Process: Z t-channel

Fig. 1: Main diagrams contributing to Vector Boson Fusion production of $WW^{(*)}$

$t\bar{t}$. To suppress non-VBF processes, the two jets are required to have $\Delta\eta_{jj} > 5.0$ and $m_{jj} > 2$ TeV. Finally, to further suppress $Z \to \tau\tau$, an estimate of the Z mass is constructed by decomposing the 2-d MET vector along the directions of two leptons and plotting the resulting mass.

The resulting yields for 100 TeV and 84 TeV are shown in Figure 1. Figure 2 shows the m_{jj} and $\Delta\eta_{jj}$ distributions before the final requirements on those two variables. Figure 3 shows distributions of the final sample for the transverse mass of the $e\mu\nu\nu$ system (m_T), ϕ between the two leptons, ϕ between the two jets, and the subleading

Table 1: Yields for the simulated 100 TeV sample and scaled to 84 TeV cross-sections assuming the same $30\,\mathrm{ab}^{-1}$ integrated luminosity.

Process	Yield for $30\,\mathrm{ab}^{-1}$ 100 TeV	Yield for $30\,\mathrm{ab}^{-1}$ scaled to 84 TeV
Resonant VBF $H \to WW^*$	27000 ± 700	21000 ± 500
Non-resonant VBF $qq \to qqWW$	170000 ± 13000	131000 ± 10000
Gluon Fusion $H \to WW^*$	4000 ± 1000	3200 ± 800
$t\bar{t}$	90000 ± 12000	67000 ± 14000
$Z \to \tau\tau$	23000 ± 7000	18000 ± 5000

jet p_T. The m_T is calculated as

$$m_T = \sqrt{2m_{e\mu}^2 + 2\left(\sqrt{m_{e\mu}^2 + p_{T,e\mu}^2}\sqrt{m_{e\mu}^2 + \not{E}_{\mathrm{T}}^2} - \vec{p}_{T,e\mu} \cdot \vec{\not{E}}_{\mathrm{T}}\right)} \quad (1)$$

which corresponds to ignoring the unmeasured components parallel to the beam and assuming the mass of the neutrino system is the same as the mass of the lepton system, which is valid in the limit that the W and W^* are at rest in the Higgs frame. Figure 3a shows a clear resonant peak just below the 125 GeV Higgs mass with a long tail to high m_T due to the non-resonant Higgs processes (Figure 1b). Figure 3c shows the classic preference for small $\Delta\phi_{e\mu}$ values due to the spin correlations of the W and W^* in the $H \to WW$ process. There is also an enhancement at large $\Delta\phi_{e\mu}$, which is correlated with the large m_T (non-resonant Higgs) region).

4 Fitting Results

The m_T distribution of the selected sample is then fit for the fractions of Higgs to $WW \to e\nu\mu\nu$ and non-resonant VBF $qq \to WW \to e\nu\mu\nu$. To exploit that the resonant Higgs signal is primarily at low $\Delta\phi_{e\mu}$ and m_{em}, and high $p_T, e\mu$ due to the scalar nature of the Higgs boson, the sample is divided into a Higgs-like and a non-Higgs-likes signal regions for fitting. The Higgs-like signal region, which has the primary effect of constraining the numerator, requires $\Delta\phi_{e\mu} < 0.8$ and $m_{e\mu} < 50\,\mathrm{GeV}$, and high $p_{T,e\mu} > 60\,\mathrm{GeV}$. The non-Higgs-like SR is the remainder of the selected events and primarily constrains the denominator. This use of regions also separates backgrounds, that primarily affect the non-resonant region, from the resonant Higgs region.

A pseudo data sample is constructed by summing all the modeled contributions and Poisson fluctuating them. A fit is then performed for a fraction of each contribution, holding gluon fusion $H \to WW^*$ and $t\bar{t}$ constant, assuming that their normalizations would be constrained from control regions. For instance, $t\bar{t}$ could be constrained by loosening the central-jet veto to allow one low-p_T b-tagged jet. The gluon fusion $H \to WW^*$ could be constrained by loosening either the central-jet veto or the m_{jj} or using multiple control regions in an ABCD method for increased robustness.

The fit setup is shown in Figure 4. The resulting expected statistical uncertainty on the ratio of resonant VBF $H \to WW^*$ to non-resonant VBF $qq \to qqWW$ is 1.8%

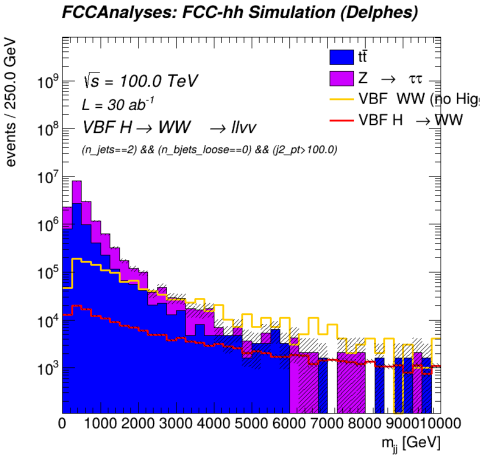

(a) Mass of the dijet system

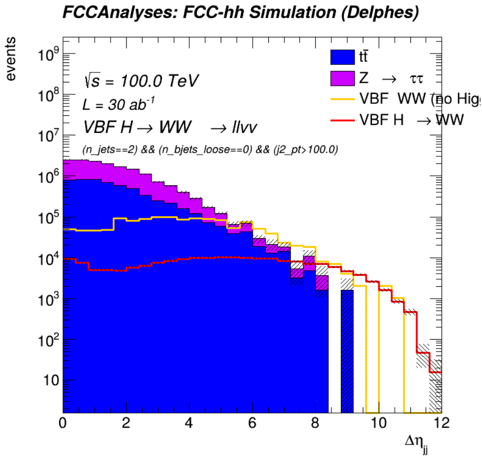

(b) Pseudorapidity difference of the jets

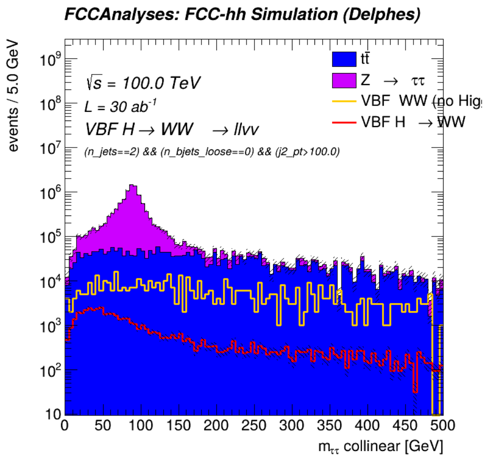

(c) Colinear estimation of $\tau\tau$ mass

Fig. 2: Distributions after the jet p_T, jet veto, and b-jet veto. The $Z\tau\tau$ and $t\bar{t}$ backgrounds are stacked while the to VBF signals are not stacked.

for 100 TeV and 1.9% for 84 TeV (both at $30\,\text{ab}^{-1}$). If $t\bar{t}$ is allowed to float in the fit to reflect that only the shape is determined for control regions the uncertainty on the ratio increases by 5% of itself. However, it is critical that the Gluon Fusion $H \to WW^*$ is constrained as m_T and $\Delta\phi_{e\mu}$ do not distinguish it from the VBF signal.

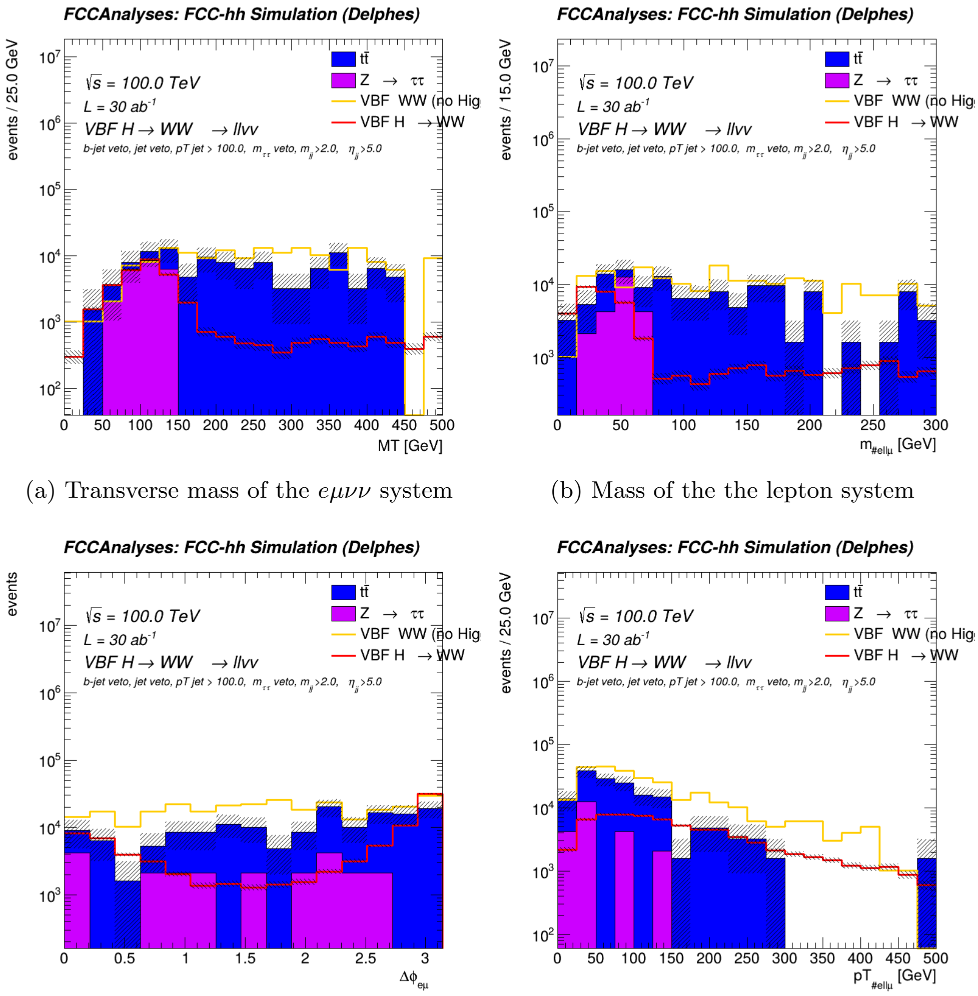

(a) Transverse mass of the $e\mu\nu\nu$ system

(b) Mass of the the lepton system

(c) ϕ between the two leptons

(d) p_T of the two leptons

Fig. 3: Distributions after the full selection including the m_{jj}, $\Delta\eta_{jj}$, and $m_{\tau\tau}$. The $Z\tau\tau$ and $t\bar{t}$ backgrounds are stacked while the two VBF signals are not stacked.

5 Conclusion

A 1.8% level sensitivity to the absolute normalization of the Higgs-coupling scale is demonstrated. A more sophisticated machine-learning-based approach plus a fit that differentiates more regions that have different signal-to-background ratios, as is often implemented for current LHC analyses, would likely improve upon this. Furthermore, more sophisticated reconstruction, specifically using tracking, could suppress the $t\bar{t}$ background, and including the same-flavor $WW^* \to \ell\nu\ell\nu$ could increase the yield.

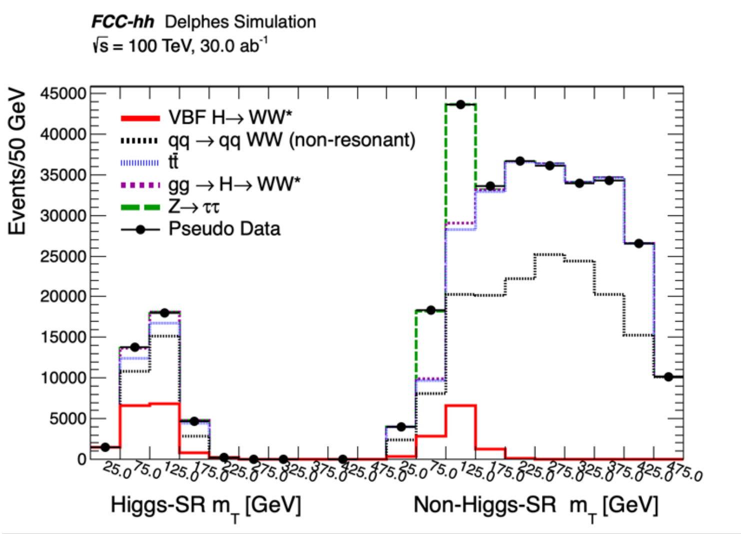

Fig. 4: Fit results to pseudo data with the m_T distribution split into Higgs-like SR and non-Higgs-like SR (see text).

Such improvements would probably lead the full sensitivity on the ratio to be in the 1-2% range, and the corresponding κ-scale sensitivity to be 0.5-1%.

Acknowledgments

This work has been partly supported by the Future Circular Collider Innovation Study (FCCIS) project, that has received funding from the European Union's Horizon 2020 research and innovation programme under grant No 951754. This material is based upon work supported by the U.S. Department of Energy, Office of Science, Office of High Energy Physics, under Award Number DE-SC0007901.

References

[1] A. Abada, et al., FCC Physics Opportunities: Future Circular Collider Conceptual Design Report Volume 1. Eur. Phys. J. C **79**(6), 474 (2019). https://doi.org/10.1140/epjc/s10052-019-6904-3

[2] T. Barklow, K. Fujii, S. Jung, R. Karl, J. List, T. Ogawa, M.E. Peskin, J. Tian, Improved Formalism for Precision Higgs Coupling Fits. Phys. Rev. D **97**(5), 053003 (2018). https://doi.org/10.1103/PhysRevD.97.053003. arXiv:1708.08912 [hep-ph]

[3] S. Di Vita, C. Grojean, G. Panico, M. Riembau, T. Vantalon, A global view on the Higgs self-coupling. JHEP **09**, 069 (2017). https://doi.org/10.1007/JHEP09(2017)069. arXiv:1704.01953 [hep-ph]

[4] M. Mangano, Higgs Physics Potential of FCC-hh Standalone. Tech. rep., CERN, Geneva (2019). URL https://cds.cern.ch/record/2681378

[5] J. Alwall, R. Frederix, S. Frixione, V. Hirschi, F. Maltoni, O. Mattelaer, H.S. Shao, T. Stelzer, P. Torrielli, M. Zaro, The automated computation of tree-level and next-to-leading order differential cross sections, and their matching to parton shower simulations. JHEP **07**, 079 (2014). https://doi.org/10.1007/JHEP07(2014)079. arXiv:1405.0301 [hep-ph]

[6] T. Sjöstrand, S. Ask, J.R. Christiansen, R. Corke, N. Desai, P. Ilten, S. Mrenna, S. Prestel, C.O. Rasmussen, P.Z. Skands, An introduction to PYTHIA 8.2. Comput. Phys. Commun. **191**, 159 (2015). https://doi.org/10.1016/j.cpc.2015.01.024. arXiv:1410.3012 [hep-ph]

[7] de Favereau, J. and Delaere, C. and Demin, P. and Giammanco, A. and Lemaître, V. and Mertens, A. and Selvaggi, M., DELPHES 3, A modular framework for fast simulation of a generic collider experiment. JHEP **02**, 057 (2014). https://doi.org/10.1007/JHEP02(2014)057. arXiv:1307.6346 [hep-ex]

[8] M. Selvaggi, A Delphes parameterisation of the FCC-hh detector. Tech. rep., CERN, Geneva (2020). URL https://cds.cern.ch/record/2717698

[9] R. Contino, et al., Physics at a 100 TeV pp collider: Higgs and EW symmetry breaking studies (2016). https://doi.org/10.23731/CYRM-2017-003.255. arXiv:1606.09408 [hep-ph]

[10] M.L. Mangano, et al., Physics at a 100 TeV pp Collider: Standard Model Processes (2016). https://doi.org/10.23731/CYRM-2017-003.1. arXiv:1607.01831 [hep-ph]